Journal of Biomechanics 82 (2019) 46–53

Contents lists available at ScienceDirect

Journal of Biomechanics

journal homepage: www.elsevier.com/locate/jbiomech
www.JBiomech.com

Integration of hyper-compliant microparticles into a 3D melanoma tumor model

Manisha K. Shah [a], Elizabeth A. Leary [a], Eric M. Darling [a,b,c,d,*]

[a] Center for Biomedical Engineering, Brown University, RI, USA
[b] Department of Molecular Pharmacology, Physiology, and Biotechnology, Brown University, RI, USA
[c] Department of Orthopaedics, Brown University, RI, USA
[d] School of Engineering, Brown University, RI, USA

ARTICLE INFO

Article history:
Accepted 17 October 2018

Keywords:
Particle penetration
Spheroid
High-throughput
Drug delivery

ABSTRACT

Multicellular spheroids provide a physiologically relevant platform to study the microenvironment of tumors and therapeutic applications, such as microparticle-based drug delivery. The goal of this study was to investigate the incorporation/penetration of compliant polyacrylamide microparticles (MPs), into either cancer or normal human cell spheroids. Incorporation of collagen-1-coated MPs (stiffness: 0.1 and 9 kPa; diameter: 15–30 μm) into spheroids (diameter ~100 μm) was tracked for up to 22 h. Results indicated that cells within melanoma spheroids were more influenced by MP mechanical properties than cells within normal cell spheroids. Melanoma spheroids had a greater propensity to incorporate and displace the more compliant MPs over time. Mature spheroids composed of either cell type were able to recognize and integrate MPs. While many tumor models exist to study drug delivery and efficacy, the study of uptake and incorporation of cell-sized MPs into established spheroids/tissues or tumors has been limited. The ability of hyper-compliant MPs to successfully penetrate 3D tumor models with natural extracellular matrix deposition provides a novel platform for potential delivery of drugs and other therapeutics into the core of tumors and micrometastases.

1. Introduction

The mechanical properties of cells are important features to integrate into possible drug delivery vehicles (Anselmo and Mitragotri, 2017; Sen Gupta, 2016; Shah et al., 2017). Engineered, drug-loaded microparticles (MP) and nanoparticles (NPs) are currently being investigated for delivery of specific molecules or signaling cues in vitro and in vivo (Agarwal et al., 2015; Ahrens et al., 2017; Anselmo and Mitragotri, 2017; Sen Gupta, 2016). Important properties to consider for fabrication include chemical and physical characteristics, such as drug loading/release profiles, degradation rates, shape, and size (Ahrens et al., 2017; Labriola et al., 2018; Labriola et al., 2016). Recently, MP mechanical properties have become another important variable to control bioavailability and bio-distribution within tissues (Anselmo and Mitragotri, 2017).

3D multicellular spheroids have been adopted as *in vitro* model systems to study the efficacy and efficiency of MP drug delivery (Costa et al., 2016; Lovitt et al., 2014). Typical 2D experiments are limited to cell monolayers as a barrier to MP entry. Common trans-well approaches work well for assessing drug or metabolite release characteristics but are ill-suited for investigating particle uptake or penetration into multi-cellular structures. As an alternative, co-culturing MPs within spheroids has shown promise as a more *in vivo*-like condition. However, few studies have looked at MP incorporation into already formed, mature spheroids that include both cells and naturally deposited extracellular matrix (ECM). Recent *in vivo* studies highlight different strategies, such as altering particle geometry and size (Best et al., 2012; Sen Gupta, 2016) and modulating elasticity (Anselmo and Mitragotri, 2017), for achieving longer persistence or increased delivery to specific tissues. Studies of particle penetration in vitro have largely been limited to enzymatically active particle coatings, such as collagenase (Goodman et al., 2007).

The goal of this study was to investigate incorporation/penetration of compliant polyacrylamide microparticles into either mature, cancerous or non-cancerous, human cell spheroids. Melanoma was used as a disease model to examine MP penetration into micrometastases-sized cell spheroids. Incorporation of compliant MPs into 1-week old spheroids was tracked over ~20 h using a

* Corresponding author at: Brown University, 175 Meeting Street, Box G-B3, Providence, RI 02912, USA.
E-mail address: Eric_Darling@brown.edu (E.M. Darling).

https://doi.org/10.1016/j.jbiomech.2018.10.018
0021-9290/

high-content, high-throughput confocal imaging system. MP speed within the spheroid and rate of MP penetration towards the centroid were measured. Additionally, MP penetration into more mature, ECM-rich spheroids were visualized over 3 weeks.

2. Methods

2.1. Cell culture

A375 (malignant melanoma) were expanded in high glucose DMEM (DMEM-HG, HyClone), 10% FBS (HyClone), and 1% penicillin/streptomycin (P/S, HyClone). Cells were passaged at ~80% confluence using 0.25% trypsin-EDTA (HyClone, GE Healthcare). HEM-L158 (HEM, human epidermal melanocytes), were expanded in Medium 254 (M254500, Gibco), 1% human melanocyte growth supplement-2 (S0165, Gibco), and 1% P/S. HEM cells were subcultured at 60–80% confluence using 0.05% Trypsin-EDTA (25300054, Gibco), followed by neutralization with Trypsin Neutralizer Solution (R002100, Gibco). All cells were maintained in humidified incubators at 37 °C, 5% CO_2.

2.2. Fabrication of MPs

Polyacrylamide MPs were fabricated using an inverse emulsion polymerization protocol as previously described, with minor modifications (Labriola et al., 2016). Mechanically distinct MPs were created with either 4% acrylamide: 0.05% bis-acrylamide ("soft") or 8% acrylamide: 0.3% bis-acrylamide ("stiff") solutions (Bio-Rad, Hercules, CA). MPs were serially filtered with 40, 30, 20, and 15 μm mesh filters to decrease size dispersity. A triphenylmethane-based highlighter dye (Sharpie) with emission at 647 nm wavelength was added for visualization. MPs were subsequently functionalized by UV-photoactivation of a heterobifunctional cross linker, sulfo-SANPAH (#13414, CovaChem), followed by overnight incubation at 4 °C in a 100 μg/mL solution of collagen type 1 (COL-1, #08-115, Lot #2373345, Millipore). Uncoated MPs were used as controls.

2.3. Mechanical characterization of MPs and cells

The elastic modulus of MP batches and cell lines were characterized with an MFP-3D-Bio atomic force microscope (AFM, Asylum Research, Santa Barbara, CA). Spherically tipped cantilevers were made by adhering 5 μm polystyrene beads to the end of silicon nitride, triangular cantilevers (Bruker Corporation, MLCT-O10, k ~ 0.03 N/m). MPs were non-specifically adhered to uncoated glass coverslips in PBS and tested at room temperature. Cells attached to glass coverslips for 30 min prior to testing in their spherical morphology using established techniques (Darling et al., 2006; Dimitriadis et al., 2002; Labriola et al., 2016). Briefly, the elastic modulus ($E_{elastic}$) of MPs and cells was determined using a thin-layer Hertz model from force versus indentation curves. Approach velocity was maintained at 10 μm/sec, and trigger forces ranged from 1 to 2 nN to achieve 1–2 μm of indentation into MPs or cells.

2.4. Spheroid formation and observation

For MP tracking experiments, a custom mold compatible with 96-well plates was fabricated with a series of 4 rows × 8 columns of pegs, each having four conical-shaped microposts (Greiner bio-one, #655891) (Leary et al., 2018). To create non-adherent hydrogels, 90 μL of sterile 2% weight/volume molten agarose (Fisher Scientific) in phosphate buffered saline (PBS) was pipetted into each well, followed by placement of the mold. Hydrogels solidified for 15 min at room temperature before removing the mold, followed by overnight equilibration in 150 μL of DMEM-HG or Medium 254 base media supplemented with 1% P/S. HEM spheroids were seeded at 400 cells/well in 20 μL of medium (100 cells/spheroid), while A375 spheroids were seeded at 200 cells/well (50 cells/-spheroid) to account for their higher proliferation rates. 30 min after cell seeding, each well was gently flooded with 150 μL of cell-specific growth medium. Media were changed every other day.

After a 7-day maturation period, culture media were removed and forty "soft" or "stiff" MPs were added to each well in 20 μL of PBS supplemented with 1% P/S (v/v) and 10 μg/mL Wheat Germ Agglutinin, Alexa Fluor 488 Conjugate (WGA, W11261, Molecular Probes, Thermo Fisher Scientific), which fluorescently labeled cells. Twenty minutes after adding this solution, wells were gently flooded with 150 μL of cell type-specific growth media.

Each well containing four spheroids was imaged using an Opera Phenix™ High Content Screening System (PerkinElmer, Waltham, MA) for up to 22 h at either 34.5, 44, or 46-minute time intervals and 10–12.5 μm z-stacks using a 20X water objective with two excitation lasers: 488 nm for WGA and 640 nm for red dye-stained MPs.

2.5. Data analysis in Imaris

Time-lapse, confocal z-slice images obtained using the Opera Phenix were analyzed using Imaris (BitPlane, Belfast, UK). Confocal slices were rendered as 3D projections, and the "Cell Detection" and "Surface Detection" software modules identified and tracked spheroid and relative MP position, respectively, in the x-y-z planes. Initial MP-spheroid contact was identified as time "0." MP position throughout the experiment was tracked using the spheroid centroid as a reference point. Due to gravity and the conical shape of the agarose molds, spheroids were typically more oval-shaped; however, for analysis of MP position, spheroids were assumed to be spherical. Spheroids with no MPs or greater than two MPs were excluded from analysis.

2.6. Assessment of MP movement

To evaluate MP incorporation based on stiffness for normal and cancerous cell types, MP position relative to spheroid centroid was tracked. Rate of penetration was determined by calculating the distance of the MP from the centroid at every time point using the distance formula:

$$AB = \sqrt{(x_2 - x_1)^2 + (y_2 - y_1)^2 + (z_2 - z_1)^2}/(t_2 - t_1)$$

where AB is the distance between the centroid of the spheroid (x_1, y_1, z_1) and the position of the MP (x_2, y_2, z_2), divided by the time, t, between measurements. MP position was normalized by spheroid radius to account for spheroid size effects. Normalized slopes tracking MP position relative to spheroid centroid at each time point for each condition (cell type and MP stiffness) were averaged to determine the rate of MP penetration. MP movement per hour (speed) was calculated for each spheroid type and MP stiffness. Linear MP movement was assumed between each time interval. Calculations included adjustments for whole-spheroid, translational movement, but rotational movement could not be tracked and was assumed negligible. Non-normalized MP rates of penetration were also calculated (Supplemental Text).

2.7. Effect of spheroid maturity

To determine whether ECM presence affected MP penetration, spheroids were cultured for up to three weeks before introducing MPs. For these experiments, cells were seeded in 96-microwell arrays made using 2% agarose (as described above) and 3D Petri

Dish® molds (24–96-Small, Microtissues Inc.). Arrays were cured for 15 min at room temperature, transferred to a 24-well plate, and equilibrated in 1% P/S, DMEM-HG overnight. HEMs were seeded at 9,600 cells/well (100 cells/spheroid), and A375 cells were seeded at 4,800 cells/well (50 cells/spheroid) to account for their higher proliferation rates. Soft and stiff MPs were added after set maturation periods: 1, 2, and 3 weeks. 48 h after adding MPs, spheroids were fixed overnight in 4% paraformaldehyde then stained with 10 μg/ml WGA and 4′,6-diamino-2-phenylindole (DAPI, Thermo Fisher), followed by imaging with an Olympus FV1000-MPE multiphoton laser scanning microscope. All images were taken using a 25x water objective and 2 μm slices.

In parallel with the above imaging experiments, cell-only spheroids were grown and collected for histological assessment of ECM deposition. At 1, 2, and 3 weeks, agarose microwells containing fixed samples were gently immersed in 100% ethanol. After overnight dehydration, the microwells were back-filled with 2% molten agarose to encapsulate spheroids in place. Samples were then embedded in paraffin, sectioned in 7 μm slices, and stained with hematoxylin and eosin (H&E) to visualize cells and ECM deposition over time.

2.8. Statistical analysis

All statistical analyses were performed using GraphPad Prism 7 (GraphPad Software, Inc). Unpaired t-tests were used to compare elastic moduli and size of cells and MPs. A one-way ANOVA was run on cell elastic modulus data, with Tukey's post-hoc analysis. Two-way ANOVAs comparing cell-type vs. MP stiffness were performed to assess differences in rate of MP penetration, followed by Tukey's post-hoc analysis. Normalized average MP position relative to spheroid centroid over time and total MP distance traveled were generated in Microsoft Excel with standard deviations. Histograms depicting MP speed within each cell type/MP type grouping were generated in Statistica, Version 13, and average MP speed data were analyzed using a two-way ANOVA, comparing cell type and MP stiffness, with Tukey HSD post-hoc test. For all statistical analyses, significance was achieved at $p < 0.05$.

3. Results

3.1. Mechanical and size characterization of HEMs, A375, and MPs

Cells and MPs were mechanically characterized using AFM. Spherical HEMs (normal melanocyte) and A375 (malignant melanoma) cells exhibited elastic moduli of ~1 kPa, though A375s were on average less compliant than HEMs ($p = 0.003$). Based on these data, MPs were fabricated to be an order of magnitude more and less compliant than the living cell types (Fig. 1A), resulting in significantly different "soft" and "stiff" MPs with elastic moduli of 0.11 ± 0.02 kPa and 9.3 ± 2.6 kPa ($p < 0.0001$), respectively. Cells were approximately 15 μm in height ($p = 0.33$), while soft and stiff MPs ranged in size from 15 to 30 μm, with the soft MPs being larger than stiff MPs ($p = 0.0011$, Fig. 1B).

3.2. Rate of penetration of MPs towards centroid of spheroids

Successful incorporation of COL-1-coated soft and stiff MPs was observed in both HEM and A375 spheroids after one week of maturation (Fig. 2). Spheroid radius-normalized average MP position over time as they were shuttled towards the centroid of A375 (Fig. 2A and B) and HEM (Fig. 2C and D) spheroids depicted greater differences in rate of soft MPs compared to stiff MPs. The average rate of soft MP penetration into A375 or HEM spheroids was approximately four times that of stiff MPs into HEM spheroids ($p < 0.05$, Fig. 2E). Rate of stiff MP penetration into A375 spheroids was approximately half that of soft MPs; however, due to the large variation, this was not significant (Fig. 2E). Uncoated MPs were not taken up by spheroids for any condition or group.

3.3. Distance traveled per interval and speed of MP within the spheroid

MPs traveled at different speeds within A375 and HEM spheroids (Fig. 3). By plotting histograms of MP distance traveled between set imaging intervals, reported as movement/hour, the diversity in this behavior could be visualized. In general, there were broader distributions for distance traveled by MPs in A375 spheroids compared to HEM spheroids, although all groups had their highest counts in the 20–50 μm/hr range (Fig. 3A–D). While no significance difference in MP speed was observed due to their stiffness, MPs within A375 spheroids were found to move faster than those within HEM spheroids ($p < 0.05$, Fig. 3E). Average speed was ~50% greater in A375 spheroids compared to HEM spheroids for soft MPs and ~25% greater for stiff MPs (Fig. 3E).

3.4. Time lapse imaging of soft MP incorporation in A375 spheroids

3D projections of confocal z-slices were taken of soft MPs (stained red) incorporating into A375 spheroids (stained with WGA) over 22 h at 44-minute intervals (Fig. 4). Introduced MPs began outside the spheroid, as shown in Image 0 (9 h and 32 min). Uptake was rapid, with full integration observed by Image 1 (10 h and 16 min). Soft MPs were shuttled through the spheroid and deformed by neighboring cells (Fig. 4, inset). Spheroids were also observed to grossly reorganize over the 13-hour period.

3.5. MP incorporation into 1-, 2-, and 3-week old spheroids

HEM and A375 spheroids were matured for 1-, 2-, or 3-weeks prior to adding soft MPs to assess MP penetration via confocal

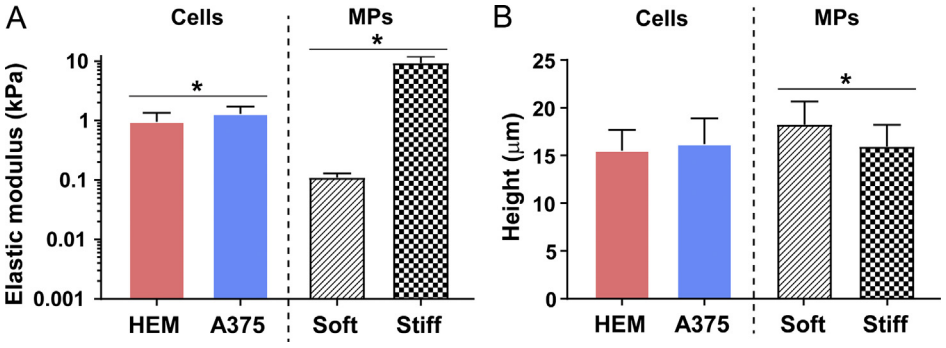

Fig. 1. Mechanical characterization of living cells and MPs. **(A)** Cells and MPs were mechanically assessed, with MP types being an order of magnitude below or above the average elastic moduli of the cells. **(B)** MPs were fabricated and filtered to be similar in size to cells in their spherical morphology. Data shown as mean ± S.D (*$p < 0.05$).

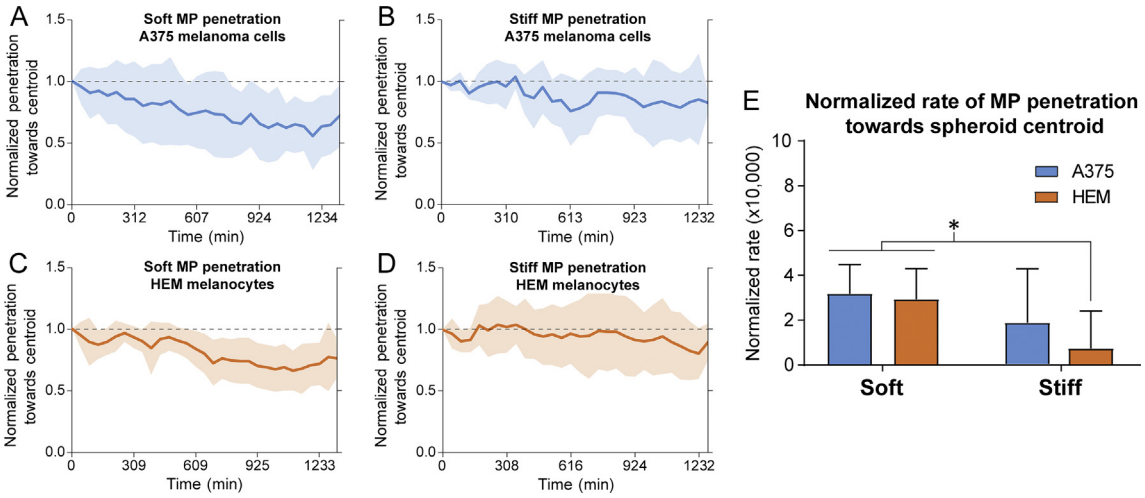

Fig. 2. MPs penetrated toward the centroid of cancer/A375 and normal/HEM spheroids at different rates. The normalized average MP position within spheroids over time showed slight differences between soft and stiff MPs interacting with (A, B) A375 and (C, D) HEM cell types (HEM/soft: n = 13, HEM/stiff: n = 7, A375/soft: n = 16, A375/stiff: n = 6). Shaded regions represent ±1 S.D. at each time point. (E) Average MP penetration rate towards the centroid of spheroids depended on MP compliance and spheroid cell type. Soft MPs were shuttled towards the centroid of the A375 and HEM spheroids at a faster rate than stiff MPs in HEM spheroids. Data shown as mean ± S.D ($^*p < 0.05$).

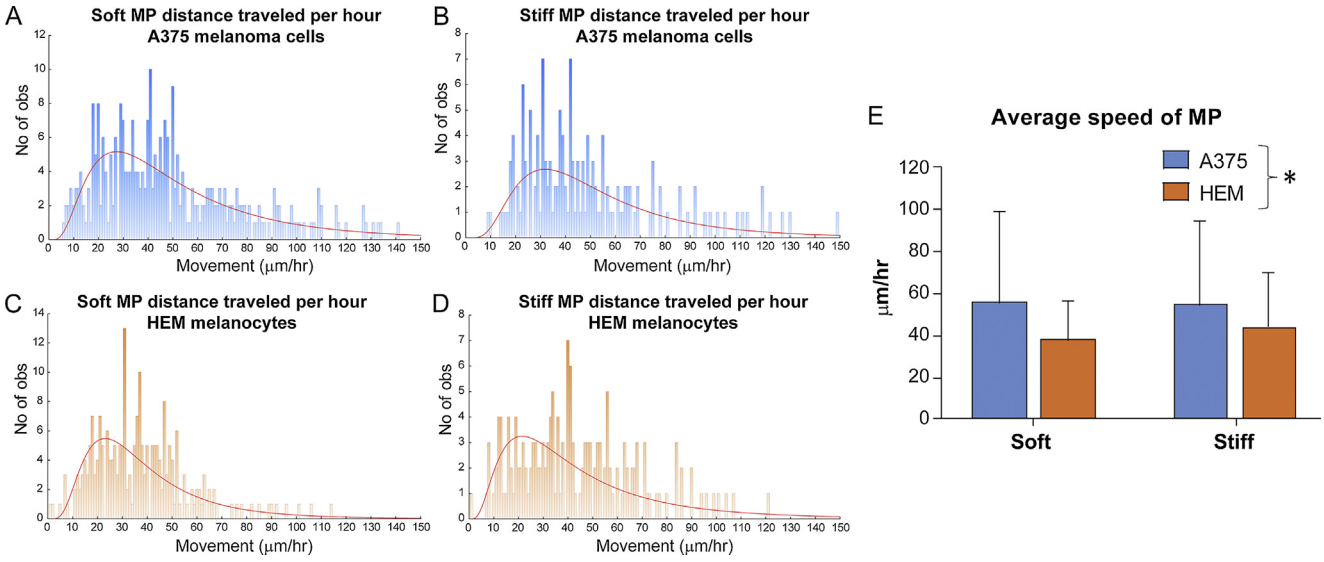

Fig. 3. Assessment of MP distance traveled per hour interval and average speed within HEM and A375 spheroids. (A-D) Histograms of the distribution of MP distance traveled per hour. Extreme outliers (>150 μm/hour) are not shown on graphs. (E) Calculations of average speed indicated that soft MPs moved more quickly in A375 spheroids than HEM spheroids. Data shown as mean ± S.D. ($^*p < 0.05$ for cell type as a factor). No of obs = Number of observations.

imaging. Samples lacking MPs (cell-only spheroids) were assessed in parallel for ECM deposition by histology. A375 cells at the 1-week time point showed cohesive spheroid formation and successful soft MP incorporation (Fig. 5A). A375 spheroids at the 2- and 3-week time points exhibited characteristics of cell death based on histological stains. Confocal imaging showed ruptured nuclei through diffuse DAPI staining. HEM spheroids remained healthy over 3 weeks, showing both matrix deposition and increased melanin production over time with concurrent soft MP incorporation (Fig. 5B).

4. Discussion

Results indicated that material mechanical properties influence cell-microparticle interactions in melanoma spheroids to a greater degree than normal melanocyte spheroids, providing increased understanding of particle penetration into ECM-rich cell spheroids. Soft MPs ($E_{elastic} \sim 0.1$ kPa) exhibited a greater propensity to incorporate into both malignant melanoma (A375) and normal melanocyte (HEM) spheroids, compared to incorporation of stiff MPs ($E_{elastic} \sim 9$ kPa) into melanoma spheroids. No difference was observed for incorporation of stiff MPs in melanoma or melanocyte spheroids. Lastly, COL-1-coated MPs were capable of penetrating spheroids matured for 1, 2, and 3 weeks.

On average, MPs were incorporated to a greater degree in melanoma spheroids compared to normal melanocyte spheroids. Typically in 2D, normal cell types have a greater affinity to migrate towards stiffer substrates, known as durotaxis (Lo et al., 2000). However, cancer cell types have been shown to lose their stiffness sensing ability upon metastasis, and thus, do not abide by typical

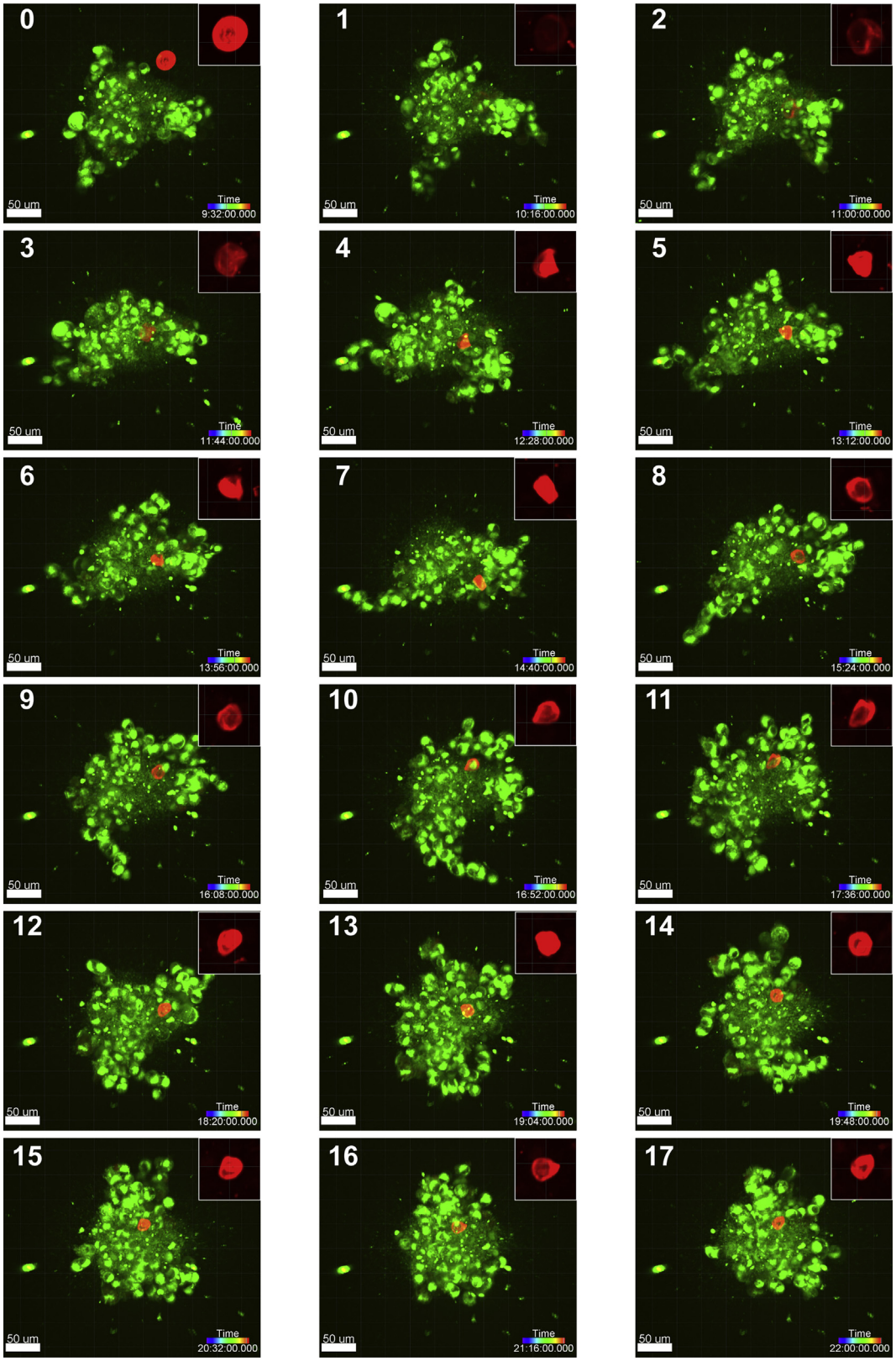

Fig. 4. Confocal 3D projections of a representative soft MP incorporating into a 7-day old A375 spheroid, with images taken at 44-minute intervals (MP: red, cells: green; scale bar = 50 μm; rainbow bar = time progression). The soft MP first interacts with and integrates into the spheroid between hour 9 and 10 of imaging (panels 0 and 1) and continues to be moved within the spheroid through hour 22. Insets (50 μm × 50 μm) depict the substantial deformation of soft MPs. Images with the MP outside and not interacting with the spheroid (< 9.5 h, panel 0) were not included in the figure. (For interpretation of the references to colour in this figure legend, the reader is referred to the web version of this article.)

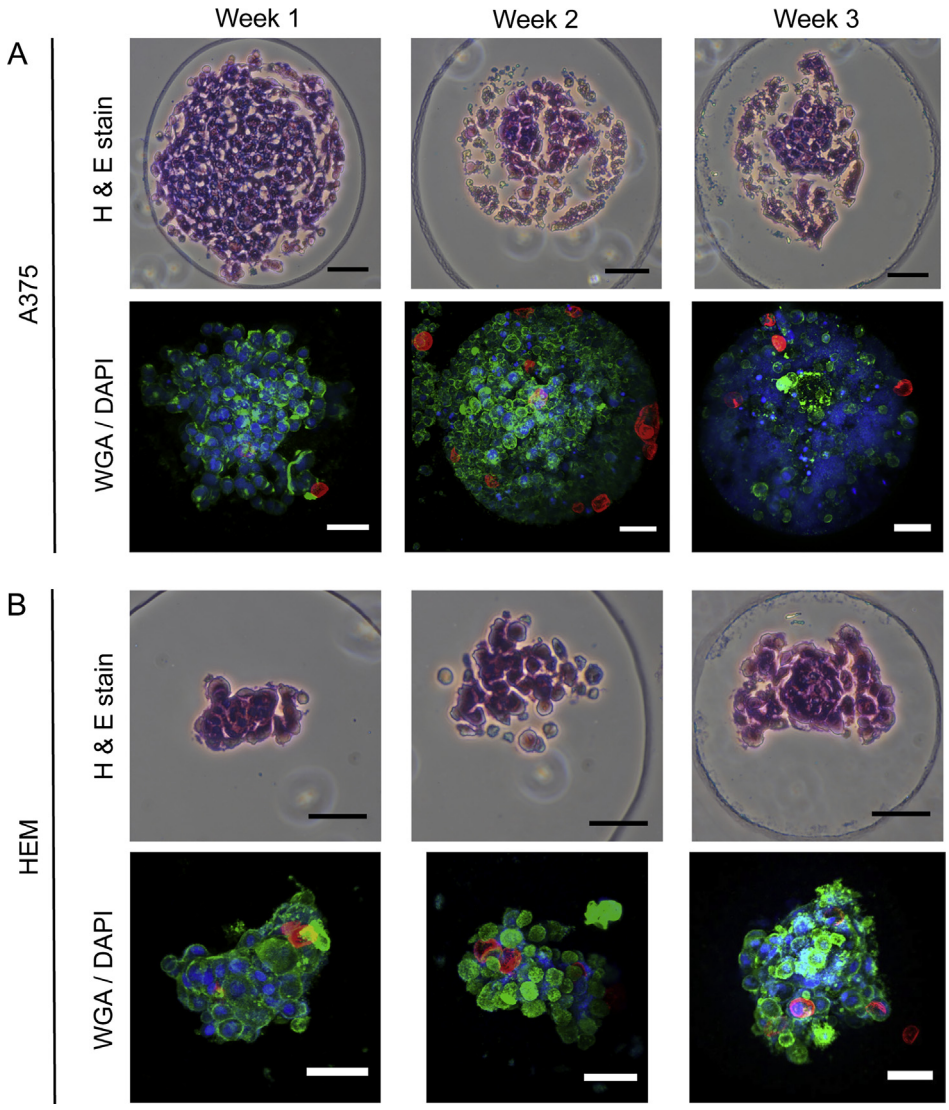

Fig. 5. Histology (cell-only spheroids) and confocal imaging (spheroids with soft MPs) of HEM and A375 spheroids over 3 weeks. (A) A375 spheroids successfully incorporated soft MPs after a 1-week maturation period. At the 2- and 3-week time points, A375 spheroids exhibited features associated with cell death possibly induced by the continued proliferation and crowding that could limit nutrient diffusion into the centroid of the spheroids. (B) HEM spheroids that were matured for up to 3 weeks prior to adding MPs exhibited matrix and melanin deposition (black dots). MPs added to the HEM spheroids after 1, 2, and 3-week maturation periods successfully incorporated. (Scale bar = 50 μm).

durotaxis theories (Chin et al., 2016; Lin et al., 2015). Compared to healthy cell types, cancer cells have been shown to exhibit increased motility on compliant substrates (300 Pa) (Lam et al., 2014). Additionally, their transformation to a more compliant phenotype allows malignant cells to become more motile regardless of the surrounding ECM stiffness. This mechanophenotype is linked to their ability to intravasate into blood vessels and metastasize (Weder et al., 2014). We hypothesize that in the current model system the more motile melanoma cells adhere to and move MPs past them at faster rates, as if the cells were trying to crawl through the spheroid using MPs and other cells as anchor points. Supplementary experiments explored this hypothesis further using normal human fibroblasts (NHF), confirming more limited MP penetration in normal cell type spheroids (Supplemental Text and Supplemental Fig. 1).

This study demonstrated that MP mechanical properties allow for divergent behaviors in melanoma versus normal spheroids. Soft MPs underwent substantial deformation by cellular forces within spheroids, while stiff MPs exhibited limited or no deformation. This hyper-compliance (<1 kPa) could play an important role for in vivo biodistribution and bioavailability of larger MPs. The vast majority of past MP/NP studies used hard polymer materials many orders of magnitude stiffer than living cells (or the MPs used in the current work). Particle sizes studied previously range from nanometers up to hundreds of micrometers. NPs used in vitro have shown internalization into individual cells through phagocytosis or endocytosis, and while these NPs have shown an ability to penetrate tissues in vivo, they tend to have short circulation times and accumulate in the spleen, lung, and kidneys (Anselmo and Mitragotri, 2017; Sen Gupta, 2016). Alternatively, MPs are not internalized by cells due to their larger size and instead interact though cell-MP binding in co-culture models (Ahrens et al., 2017). However, penetration into tissues and sustained circulation in vivo without occluding small vessels is limited, particularly for MPs made of rigid materials. In vivo studies with hyper-compliant MPs have yet to be done, but results using materials in the ~10 kPa range have indicated that an increase in circulation time is possible (Anselmo et al., 2015). The current work suggests

additional benefits might exist when soft MPs interface with cell/ECM structures. Their deformability facilitates increased movement, whereas less compliant MPs may induce more stable interactions through focal adhesion development and binding at cell-substrate interfaces, limiting displacement of stiff MPs (Discher et al., 2005; Yeung et al., 2005). Supplemental experiments assessing incorporation of much stiffer, COL-1-coated polystyrene (PS) MPs into melanoma versus normal cell spheroids revealed limited penetration (Supplemental Text and Supplemental Figs. 1 and 2), similar to stiff MPs. Based on our results, adding compliance as an important MP material property could help bridge the gap between current NP and MP studies as a means for particle penetration into native cell/ECM structures or tumors.

The present study showed that MPs 15–30 μm in size successfully penetrated pre-established melanoma and normal cell spheroids (Supplemental Fig. 3). A balance between fabricating MPs small enough to increase circulation time and prevent entrapment in capillary and alveolar vessels, while large enough that they will not be phagocytosed, is an important consideration. Based on literature, decreasing the size of the current MPs to mimic blood cell size of 5–7 μm could allow for increased circulation time allowing for margination and extravasation from blood vessels into tissues (Anselmo and Mitragotri, 2017; Sen Gupta, 2016). It can further be argued that instead of the internalization of a particle into a cell, as seen with particles <5 μm in diameter (Agarwal et al., 2015; Barua and Mitragotri, 2014; Beningo and Wang, 2002; Champion et al., 2008; Sen Gupta, 2016), the ability of an MP to be moved around and spread throughout a spheroid would allow for increased, consistent drug delivery to the whole tumor using fewer MPs.

While signaling molecules and matrix metalloprotease (MMP) expression were beyond the scope this study, the penetration of COL-1-coated MPs could be due to an induction of ECM degradation and cell migration mechanisms. The role of cadherins and integrins in normal melanocytes versus melanoma is a growing field. Specifically, normal melanocytes express E-cadherins to maintain communication with neighboring keratinocytes, which help downregulate expression of the $\alpha_v\beta_3$ integrin, an integrin linked to cancer progression and other diseases (Haass et al., 2005). However in melanoma, E-cadherin is downregulated, with concurrent upregulation of N-cadherin, $\alpha_v\beta_3$, $\alpha IIb\beta_3$, and $\alpha_4\beta_1$ to allow melanoma cells to communicate with underlying fibroblasts and eventually endothelial cells to enter vasculature (Haass et al., 2005; Kuphal et al., 2005; Trikha et al., 1997; van der Flier and Sonnenberg, 2001). In particular, $\alpha_v\beta_3$ is a promiscuous integrin, with the ability to bind many ligands and upregulate expression of MMP-1 and activation of MMP-2, which degrades collagen matrix and promotes melanoma cell migration (Natali et al., 1993; Ntayi et al., 2001). As collagen matrix is broken down by MMPs, expression of $\alpha_v\beta_3$ allows for continued binding to this non-fibrillar or denatured collagen (Henriet et al., 2000). Combined, this could explain differences observed in the degree of soft MP integration and reorganization within melanoma versus melanocyte spheroids.

The cell types used in this study exhibited different proliferation rates, with A375 cells dividing more quickly than HEM or NHF cells. This led to HEM and NHF spheroids being about half the size of A375 spheroids. To help account for these differences, MP penetration data were normalized by spheroid radius to determine if this characteristic influenced MP movement. These normalized results showed differences in MP penetration based on elastic modulus. However, when analyzing non-normalized data, average MP penetration rate towards the centroid of spheroids depended on MP compliance and spheroid cell type (Supplemental Fig. 4), with soft MPs being shuttled towards the centroid of the A375 spheroids at a faster rate than in HEM spheroids. Further experiments accounting for proliferation, cell size, and spheroid size could provide deeper insight into the role of these parameters.

This study is among the first to visualize MP penetration into developed, mature spheroids, identifying hyper-compliance as a key factor for penetration. This property not only facilitated initial incorporation of MPs into the spheroid but also increased displacements within melanoma spheroid models. Additional modifications to these MPs may allow the targeting of specific tissues in the future, and adoption of a highly compliant, biodegradable polymer material would facilitate more effective, drug delivery options. Ultimately, this study helps inform development of novel, therapeutically-relevant MPs for drug delivery applications within cancer, and potentially a range of other pathologies.

Author contributions

M.K.S and E.M.D. designed the study, analyzed data, and wrote the manuscript. M.K.S. performed all experiments. E.A.L. assisted with experiment set up and data analysis. All authors gave final approval for publication.

Acknowledgements

The authors would like to thank Elena Oancea for discussions on melanoma and the Center for Predictive Biology for use of the Opera PhenixTM. Thank you to Benjamin Wilks, Kali Manning, and Jeffrey Morgan for guidance with making spheroids and further analysis. Thank you to Vera Fonseca for help with staining spheroids, and Jessica Sadick, Rafael González Cruz, and Nicholas Labriola for useful discussions on data analysis. This work was supported by awards from the National Institute of Health (R01 AR063642, P20 GM104937) and the National Science Foundation (CAREER CBET 1253189). The content of this article is solely the responsibility of the authors and does not necessarily represent the official views of the National Science Foundation or National Institutes of Health.

Conflict of Interest

EMD has an equity interest in MimicSphere, LLC. This relationship has been reviewed and managed by Brown University in accordance with its conflict of interest policies.

Appendix A. Supplementary material

Supplementary data to this article can be found online at https://doi.org/10.1016/j.jbiomech.2018.10.018.

References

Agarwal, R., Jurney, P., Raythatha, M., Singh, V., Sreenivasan, S.V., Shi, L., Roy, K., 2015. Effect of shape, size, and aspect ratio on nanoparticle penetration and distribution inside solid tissues using 3D spheroid models. Adv. Healthc. Mater. 4, 2269–2280.

Ahrens, C.C., Dong, Z., Li, W., 2017. Engineering cell aggregates through incorporated polymeric microparticles. Acta Biomater. 62, 64–81.

Anselmo, A.C., Mitragotri, S., 2017. Impact of particle elasticity on particle-based drug delivery systems. Adv. Drug. Deliv. Rev. 108, 51–67.

Anselmo, A.C., Zhang, M., Kumar, S., Vogus, D.R., Menegatti, S., Helgeson, M.E., Mitragotri, S., 2015. Elasticity of nanoparticles influences their blood circulation, phagocytosis, endocytosis, and targeting. ACS Nano 9, 3169–3177.

Barua, S., Mitragotri, S., 2014. Challenges associated with penetration of nanoparticles across cell and tissue barriers: a review of current status and future prospects. Nano Today 9, 223–243.

Beningo, K.A., Wang, Y.L., 2002. Fc-receptor-mediated phagocytosis is regulated by mechanical properties of the target. J. Cell Sci. 115, 849–856.

Best, J.P., Yan, Y., Caruso, F., 2012. The role of particle geometry and mechanics in the biological domain. Adv. Healthc. Mater. 1, 35–47.

Champion, J.A., Walker, A., Mitragotri, S., 2008. Role of particle size in phagocytosis of polymeric microspheres. Pharm. Res.-Dordr. 25, 1815–1821.

Chin, L., Xia, Y., Discher, D.E., Janmey, P.A., 2016. Mechanotransduction in cancer. Curr. Opin. Chem. Eng. 11, 77–84.
Costa, E.C., Moreira, A.F., de Melo-Diogo, D., Gaspar, V.M., Carvalho, M.P., Correia, I.J., 2016. 3D tumor spheroids: an overview on the tools and techniques used for their analysis. Biotechnol. Adv. 34, 1427–1441.
Darling, E.M., Zauscher, S., Guilak, F., 2006. Viscoelastic properties of zonal articular chondrocytes measured by atomic force microscopy. Osteoarthr. Cartilage 14, 571–579.
Dimitriadis, E.K., Horkay, F., Maresca, J., Kachar, B., Chadwick, R.S., 2002. Determination of elastic moduli of thin layers of soft material using the atomic force microscope. Biophys. J. 82, 2798–2810.
Discher, D.E., Janmey, P., Wang, Y.L., 2005. Tissue cells feel and respond to the stiffness of their substrate. Science 310, 1139–1143.
Goodman, T.T., Olive, P.L., Pun, S.H., 2007. Increased nanoparticle penetration in collagenase-treated multicellular spheroids. Int. J. Nanomed. 2, 265–274.
Haass, N.K., Smalley, K.S., Li, L., Herlyn, M., 2005. Adhesion, migration and communication in melanocytes and melanoma. Pigment Cell Res 18, 150–159.
Henriet, P., Zhong, Z.D., Brooks, P.C., Weinberg, K.I., DeClerck, Y.A., 2000. Contact with fibrillar collagen inhibits melanoma cell proliferation by up-regulating p27KIP1. Proc. National Academy Sci. United States of America 97, 10026–10031.
Kuphal, S., Bauer, R., Bosserhoff, A.K., 2005. Integrin signaling in malignant melanoma. Cancer Metast. Rev. 24, 195–222.
Labriola, N.R., Azagury, A., Gutierrez, R., Mathiowitz, E., Darling, E.M., 2018. Concise review: fabrication, customization, and application of cell mimicking microparticles in stem cell science. Stem Cells Transl. Med. 7, 232–240.
Labriola, N.R., Mathiowitz, E., Darling, E.M., 2016. Fabricating polyacrylamide microbeads by inverse emulsification to mimic the size and elasticity of living cells. Biomater. Sci. 5, 41–45.
Lam, C.R., Wong, H.K., Nai, S., Chua, C.K., Tan, N.S., Tan, L.P., 2014. A 3D biomimetic model of tissue stiffness interface for cancer drug testing. Mol. Pharm. 11, 2016–2021.
Leary, E., Rhee, C., Wilks, B.T., Morgan, J.R., 2018. Quantitative live-cell confocal imaging of 3D spheroids in a high-throughput format. SLAS Technol. 2472630318756058.
Lin, H.H., Lin, H.K., Lin, I.H., Chiou, Y.W., Chen, H.W., Liu, C.Y., Harn, H.I., Chiu, W.T., Wang, Y.K., Shen, M.R., Tang, M.J., 2015. Mechanical phenotype of cancer cells: cell softening and loss of stiffness sensing. Oncotarget 6, 20946–20958.
Lo, C.M., Wang, H.B., Dembo, M., Wang, Y.L., 2000. Cell movement is guided by the rigidity of the substrate. Biophys. J. 79, 144–152.
Lovitt, C.J., Shelper, T.B., Avery, V.M., 2014. Advanced cell culture techniques for cancer drug discovery. Biology (Basel) 3, 345–367.
Natali, P.G., Nicotra, M.R., Bartolazzi, A., Cavaliere, R., Bigotti, A., 1993. Integrin expression in cutaneous malignant melanoma: association of the alpha 3/beta 1 heterodimer with tumor progression. Int. J. Cancer 54, 68–72.
Ntayi, C., Lorimier, S., Berthier-Vergnes, O., Hornebeck, W., Bernard, P., 2001. Cumulative influence of matrix metalloproteinase-1 and -2 in the migration of melanoma cells within three-dimensional type I collagen lattices. Exp. Cell Res. 270, 110–118.
Sen Gupta, A., 2016. Role of particle size, shape, and stiffness in design of intravascular drug delivery systems: insights from computations, experiments, and nature. Wiley Interdiscip Rev. Nanomed. Nanobiotechnol. 8, 255–270.
Shah, M.K., Garcia-Pak, I.H., Darling, E.M., 2017. Influence of inherent mechanophenotype on competitive cellular adherence. Ann. Biomed. Eng. 45, 2036–2047.
Trikha, M., Timar, J., Lundy, S.K., Szekeres, K., Cai, Y., Porter, A.T., Honn, K.V., 1997. The high affinity alphaIIb beta3 integrin is involved in invasion of human melanoma cells. Cancer Res. 57, 2522–2528.
van der Flier, A., Sonnenberg, A., 2001. Function and interactions of integrins. Cell Tissue Res. 305, 285–298.
Weder, G., Hendriks-Balk, M.C., Smajda, R., Rimoldi, D., Liley, M., Heinzelmann, H., Meister, A., Mariotti, A., 2014. Increased plasticity of the stiffness of melanoma cells correlates with their acquisition of metastatic properties. Nanomedicine 10, 141–148.
Yeung, T., Georges, P.C., Flanagan, L.A., Marg, B., Ortiz, M., Funaki, M., Zahir, N., Ming, W., Weaver, V., Janmey, P.A., 2005. Effects of substrate stiffness on cell morphology, cytoskeletal structure, and adhesion. Cell Motil. Cytoskeleton 60, 24–34.